Nanoscale

PAPER

View Article Online
View Journal | View Issue

Cite this: *Nanoscale*, 2019, **11**, 14720

Synthesis of $(V_{2/3}Sc_{1/3})_2AlC$ i-MAX phase and $V_{2-x}C$ MXene scrolls†

Jimmy Thörnberg, * Joseph Halim, Jun Lu, Rahele Meshkian, Justinas Palisaitis, Lars Hultman, Per O.Å. Persson and Johanna Rosen*

Received 18th March 2019,
Accepted 22nd July 2019

DOI: 10.1039/c9nr02354b

rsc.li/nanoscale

We report the synthesis and characterization of a new laminated i-MAX phase, $(V_{2/3}Sc_{1/3})_2AlC$, with in-plane chemical ordering between the M-elements. We also present evidence for the solid solution $(V_{2-x}Sc_x)_2AlC$, where $x \leq 0.05$. Chemical etching of the Al and Sc results in a two-dimensional (2D) MXene counterpart: $V_{2-x}C$ from the latter phase. Furthermore, etching with HF yields single-sheet MXene of flat morphology, while LiF + HCl gives MXene scrolls. We also show a 4× reduction in etching time for $(V_{2-x}Sc_x)_2AlC$ compared to V_2AlC, suggesting that traces of Sc changes the phase stability, and make the material more susceptible to etching. The results show a path for improved control of MXene synthesis and morphology, which may be applicable also for other MAX/MXene systems.

Introduction

Two-dimensional (2D) materials, such as graphene, BN, MoS_2 and silicene possess unique properties that differ from their 3D counterparts.[1–3] Discovered in 2011, a substantial addition to the 2D family is MXene, 2D transition metal carbides and/or nitrides,[4–6] that have led to extensive theoretical and experimental research worldwide. MXenes are obtained by selective etching of the A-layer (typically Al, Ga or Si),[4,7,8] from the atomically laminated parent $M_{n+1}AX_n$ (MAX) phases, where M is a transition metal, A is an A-group element, X is C and/or N, and n = 1–3.[9,10] To date, MXenes have shown potential for a wide range of applications, including supercapacitors, transparent conducting electrodes, electromagnetic shielding, and gas/bio sensors.[11–16] Also, MAX phases have attracted a considerable interest, with the nature of bonding being a mixture of metallic, covalent and ionic.[17] Hence, they display a combination of metallic and ceramic properties, *e.g.*, high hardness, high thermal decomposition temperature, and oxidation resistance *vs.* good electrical and thermal conductivity and good machinability.[9]

During the process of removing the A-element from the MAX phase for MXene synthesis, the emerging MXene surfaces are immediately terminated by species that are native to the etchant. Hence, MXenes are generally described by $M_{n+1}X_nT_x$, where the terminating species, T_x, constitute a combination of –O, –OH, and –F.[18,19] What renders MXenes different from other 2D materials, is their combination of high conductivity, hydrophilicity, and their chemical diversity, the latter making them tuneable through their large variation of intrinsic compositions (*e.g.*, $Ti_3C_2T_x$, Mo_2CT_x, V_2CT_x). Changing the surface terminations further adds to their variety in materials characteristics.[11,14,19,20]

The morphology of a 2D material can also be crucial for the materials properties. It has been shown that morphologies of $Ti_3C_2T_x$ MXene nanosheets can be manipulated through spray-dried droplets to form 3D crumpled structures through capillary forces.[21] There are also examples showing that $Ti_3C_2T_x$ MXene can be synthesized by acid induced crumpling,[22,23] and even form conical scrolls.[4] The latter could potentially be of high importance when using multi-stacked delaminated MXenes papers as electrode materials for applications in electrochemical energy storage.[24] The restacking of delaminated MXene puts constraints on electrolyte ion transport and may reduce the efficiency of the MXene surfaces. This problem has been thoroughly investigated for graphene used in electrodes,[25] where it has been shown that use of interlayer spacers, such as nanoparticles, nanotubes and/or nanosheets between the graphene layers, may greatly improve ion-transport in and between the layers.[24,26–29] Changing these interlayer spacers to MXene nanosheets with a manipulated morphology, has the potential to advance the boundaries of MXenes as electrode materials.

A mixture of elements on the M-, A-, and X-sites in the MAX phase increases the ability to tune the materials properties even further, realizing, *e.g.*, material strengthening and/or changes in electrical and magnetic properties.[30–32] Alloying also opens up the ability to include elements not considered in traditional ternary MAX phases.[33–35] Typically, the element

Thin Film Physics Division, Department of Physics, Chemistry, and Biology (IFM), Linköping University, SE-581 83 Linköping, Sweden. E-mail: johanna.rosen@liu.se

†Electronic supplementary information (ESI) available. See DOI: 10.1039/c9nr02354b

mixture form a solid solution, but recently, chemical ordering of M elements in quaternary MAX phases was discovered, with both out-of-plane (o-MAX)[36,37] and in-plane (i-MAX) order.[38] i-MAX phases are described by the general formula $(M^1_{2/3}M^2_{1/3})_2AX$, to date reported for the ten compositions $(Mo_{2/3}Sc_{1/3})_2AlC$, $(Mo_{2/3}Y_{1/3})_2AlC$, $(V_{2/3}Zr_{1/3})_2AlC$, $(Cr_{2/3}Sc_{1/3})_2AlC$, $(Cr_{2/3}Y_{1/3})_2AlC$, $(Cr_{2/3}Zr_{1/3})_2AlC$, $(W_{2/3}Sc_{1/3})_2AlC$, $(W_{2/3}Y_{1/3})_2AlC$, $(Mo_{2/3}Sc_{1/3})_2GaC$, and $(Mo_{2/3}Y_{1/3})_2GaC$.[38–43] These phases are similar to traditional MAX phases, with the exception of having two different transition metals, which are chemically ordered in the basal plane. A main characteristic of the minority M^2 elements is that they extend from the M layer towards the A layer, which may be of importance for the transformation into MXene. Conversion of i-MAX to MXene has been shown to realize a 2D material with in-plane chemical order, or ordered vacancies, by removal of the A-layer or the A-layer as well as the M^2 element, respectively.[38,41,44]

Herein we present synthesis and characterization of a new i-MAX phase, $(V_{2/3}Sc_{1/3})_2AlC$, and V_2AlC MAX phase alloyed with a small amount of Sc. Furthermore, we show that through choice of etching procedure it is possible to produce MXene in the form of flakes or scrolls. The results thus outline a new route for manipulation of MXene morphology, widening the range of applications.

Experimental details

For synthesis through pressureless sintering, elemental powders of V (99.5%, Alfa Aesar), Sc (99.5%, Alfa Aesar), Al (99%, Alfa Aesar) and C (99.9995%, Acros Organics), with particle sizes of 44 μm, 75 μm, 75 μm and 150 μm, respectively, were mixed in stoichiometric i-MAX ratios. The prepared powder was put in a crucible and placed into a STATF-1700X vacuum sintering furnace, with synthesis performed in Ar, at atmospheric pressure. The heating from room temperature (RT) to 900 °C, from 900 to 1500 °C (synthesis temperature, kept for 2 h), and then back from 1500 °C to 900 °C, was performed using +5, +10, and −5 °C per minute, respectively.

Synthesis of MXene was carried out using 20 ml, 10 to 48 wt% hydrofluoric acid (HF, Sigma-Aldrich), per 1 g material. Optimization was made from more than 30 sets of etching trails, varying the HF concentration from 10 to 48 wt% and the etching time from 10 to 24 h. Washing was done by diluting the solutions with DI water, manual shaking for 1 min, and then centrifuging for 2 min at 5000 rpm. At this point, the material fully settled and the diluted HF solution was disposed. This process was repeated until the pH level reached 6 or more. Delamination of the multilayered MXene was done by adding 5 ml of 40 wt% organic base, tetrabutylammonium hydroxide (TBAOH, Sigma-Aldrich) per 1 g of material, and shaking for 5 min. The mixture was centrifuged for 2 min at 5000 rpm followed by careful DI water rinsing without shaking, to not cause spontaneous delamination. This procedure was repeated three times, removing all TBAOH residues. At this point DI water was added, followed by 15 min manual shaking, 1 h of sonication and 1 h of centrifuging at 3500 rpm. Finally, the supernatant was micro-filtered onto nanoporous polypropylene membranes (Celgard 3501, 0.065 μm pore size, Celgard LLC).

Synthesis of MXene using 36 wt% hydrochloric acid (HCl, Sigma Aldrich) and lithium fluoride (LiF) was also performed, using 20 ml HCl with 2 g LiF powder per 1 g material under stirring in RT. Washing was done using similar procedures as for HF etching. Rinsing was done using 10 wt% aqueous HCl and a LiCl solution, 20 ml DI water per 1 g lithium chloride (LiCl, Sigma-Aldrich), three times, respectively. Mixtures were manually shaken for 1 min and centrifuged for 2 min at 5000 rpm. Delamination was done by adding DI water, shaking for ~10 min and centrifuging for 5 min at 3500 rpm until clear signs of supernatant occurred. Filtering of the material was done using the same procedure as for HF etching.

Trials to use NaF + HCl as etching agent was also made, including heating to 50 °C for between 2 and 48 h.

X-ray diffraction (XRD) and θ–2θ scans on the powder samples were performed using a PANalytical X'Pert powder diffractometer, with Cu source (λ = 1.54 Å). The optics utilized for these measurements were a graded Bragg–Brentano HD with $\frac{1}{2}^\circ$ divergent and $\frac{1}{2}^\circ$ antiscattered slits for the incident beam side, and a 5 mm antiscatter slit together with a Soller slit for the diffracted beam side. A 5–120° continuous scan was performed on the sample using a step size of 0.016° with a 10 s time per step.

Compositional and structural analysis was done with a scanning electron microscope (SEM) LEO 1550 Gemini equipped with an Oxford Instruments energy-dispersive X-ray (EDX) detector operating with an acceleration voltage between 5–15 keV. High resolution scanning transmission electron microscopy imaging with EDX (HRSTEM-EDX) and selective area electron diffraction (SAED) was used to determine the atomic structure, composition and crystallographic orientation of the material. Electron microscopy was performed using the Linköping double corrected FEI Titan^3 60–300 equipped with a monochromated high brightness field emission gun (XFEG), Super-X EDX detectors and a Quantum ERS-GIF. Both EDX analyses were calibrated by ZAF methods.

Results & discussion

The highest yield of $(V_{2/3}Sc_{1/3})_2AlC$ i-MAX phase, estimated from XRD combined with SEM-EDX for identification of grains with i-MAX composition, was roughly 55% and given by a stoichiometric powder composition sintered at 1500 °C, even though the phase could be observed also at 1400 and 1600 °C along with an increasing content of impurity phases, see XRD discussion below. The V_2AlC MAX phase was identified in the same temperature range.

Fig. 1(a–c) shows HRSTEM images from $(V_{2/3}Sc_{1/3})_2AlC$ i-MAX particles with in-plane orientations [010], [011], and [001], along with schematic illustrations based on a monoclinic crystal structure of $C2/c$ symmetry. The insets in the

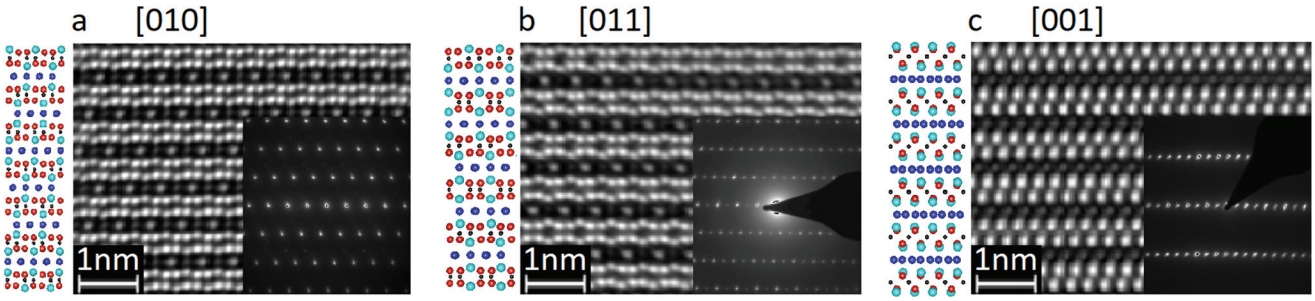

Fig. 1 HRSTEM and corresponding SAED images of $(V_{2/3}Sc_{1/3})_2AlC$ along the (a) [010], (b) [011], and (c) [001] crystal orientation, together with schematics based on a monoclinic *C*2/*c* symmetry. The red, teal, blue, and black spheres in the schematics are V, Sc, Al, and C, respectively.

images show the corresponding SAED patterns, which confirm the *C*2/*c* symmetry. Fig. 1(a and b) display an in-plane chemically ordered configuration of brighter spots of V and darker spots of Sc, where the Sc extends out from the M-plane towards the Al-layer. This is a general characteristic feature of an i-MAX phase, together with the observation of an alternating intensity the Al layer (every second Al has a weak contrast), which in turn is an indication of Kagomé-like ordering. Fig. 1(c) shows the traditional MAX phase structure, which from the crystallographic [100] direction is representative for both MAX and i-MAX. HRSTEM-EDX compositional analysis shows the expected stoichiometric 2 : 1 V : Sc ratio.

Fig. 2(a) shows a HRSTEM image from a grain of V_2AlC MAX phase present as an impurity phase in the powder sample. Some of the V_2AlC particles also have traces of Sc, estimated to be up to 5 at%, though not exceeding this amount. The Sc content was estimated using SEM + EDX of more than 100 particles chosen at random, and Fig. 2(b) shows EDX spectra of an arbitrary V_2AlC particle with traces of Sc. The observations suggest that we in the same powder sample have a mixture of stoichiometric $(V_{2/3}Sc_{1/2})_2AlC$ i-MAX, V_2AlC MAX phase, and V_2AlC MAX phase with a small concentration of Sc, onwards referred to as $(V_{2-x}Sc_x)_2AlC$ MAX. Consequently, in the here analyzed powder sample we make the distinction between these three phases, through for simplicity we refer to the overall powder sample as $(V_{2/3}Sc_{1/2})_2AlC_{mix}$. Based on SEM + EDX, pure V_2AlC MAX phase is concluded to be of lowest concentration.

XRD of $(V_{2/3}Sc_{1/3})_2AlC_{mix}$ and a corresponding simulated diffraction pattern based on a monoclinic *C*2/*c* symmetry of the i-MAX phase, as suggested from SAED and STEM analysis, is shown in Fig. 3. A majority of the peaks in the simulated spectra corresponds to the measured spectra, though with some shift at lower angles due to the constraints of the cell size used for the simulation. The traditional 110 i-MAX peak can be seen at 19.4°, corresponding to an interplanar spacing of 0.46 nm, which appear solely from the chemical ordering of the M^1 and M^2 elements.[39] In addition, the remaining peaks belong to impurity phases V_2AlC (MAX), Sc_3AlC, VC, and Al_2O_3. Note that most of the peaks from the i-MAX and the MAX phase overlaps,[31] such as at 13.4° for the 002 peak, 26.9° for the 004 peak, *etc.*

Prior to discussing derivation of MXene, it should be noted that the time to dissolve Al from V_2AlC has been reported to be

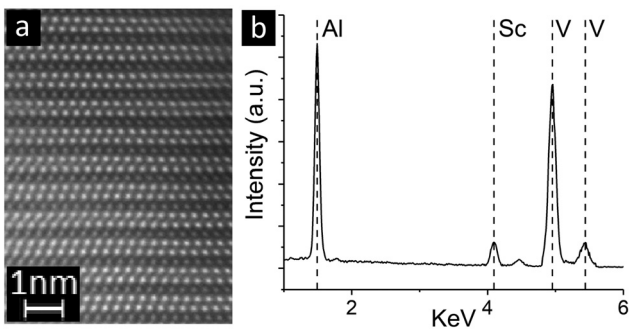

Fig. 2 (a) HRSTEM-HAADF showing the laminated structure of V_2AlC MAX and (b) corresponding SEM-EDX showing V_2AlC particles with traces of Sc up to 5 at%, also referred to as $(V_{2-x}Sc_x)_2AlC$ MAX. Both phases are present in $(V_{2/3}Sc_{1/2})_2AlC_{mix}$.

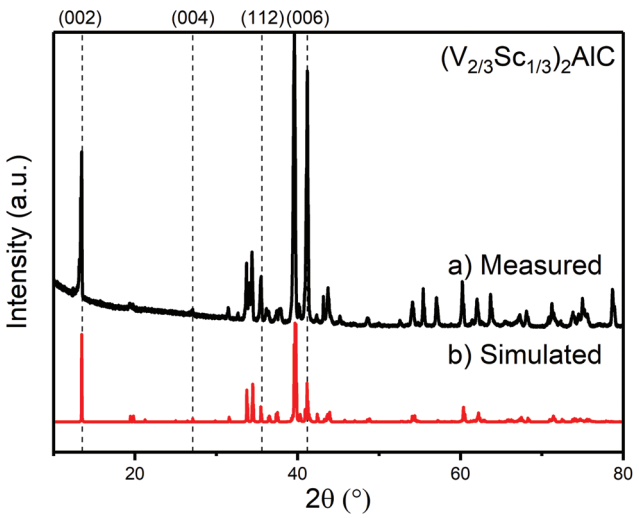

Fig. 3 (a) Measured and (b) simulated XRD pattern for $(V_{2/3}Sc_{1/3})_2AlC_{mix}$. Apart from the i-MAX phase, the measured sample show signs of V_2AlC and $(V_{2-x}Sc_x)_2AlC$ MAX phase, Sc_3AlC, VC and Al_2O_3. The simulated scan is based on an i-MAX structure of monoclinic *C*2/*c* symmetry.

Table 1 Various etchants and conditions used for MXene synthesis. The morphology of respective sample is shown in Fig. 5 and 6. Conditions for V_2AlC MAX phase taken from reference

Sample phase composition	Etching agent	Time [h]	Morphology	Comment
V_2AlC	Aqueous HF (50%)	90	Single flakes	Ref. 45
V_2AlC MAX phase $(V_{2-x}Sc_x)_2AlC$ MAX phase $(V_{2/3}Sc_{1/2})_2AlC$ i-MAX phase	Aqueous HF (48%)	24	Single flakes	i-MAX dissolved, $V_{2-x}C$ MXene + MAX.
V_2AlC MAX phase $(V_{2-x}Sc_x)_2AlC$ MAX phase $(V_{2/3}Sc_{1/2})_2AlC$ i-MAX phase	NaF + HCl	9	—	i-MAX dissolved, MAX remains.
V_2AlC MAX phase $(V_{2-x}Sc_x)_2AlC$ MAX phase $(V_{2/3}Sc_{1/2})_2AlC$ i-MAX phase	HCl + LiF	144	Single flakes, scrolls	i-MAX dissolved, $V_{2-x}C$ MXene + MAX.

90 h in HF,[45] see Table 1. For etching in HF, all here attempted sets of etching parameters dissolved the $(V_{2/3}Sc_{1/2})_2AlC$ i-MAX. The immediate reaction was strongly exothermic even at low HF concentrations (<10%), suggesting a reaction between the i-MAX and HF. However, after 24 h in 48% HF concentration, there was evidence for formation of MXene and ScF_3, see XRD in Fig. 4(a and b), showing the $(V_{2/3}Sc_{1/3})_2AlC_{mix}$ sample before and after treatment with HF and subsequent TBAOH delamination. Considering that the V_2AlC MAX phase seems to be unaffected at this point, together with the presence of the Sc-containing salt, suggests that the $(V_{2-x}Sc_x)_2AlC$ MAX phase transformed into multilayer $V_{2-x}CT_x$ MXene. The large reduction in etching time for $(V_{2-x}Sc_x)_2AlC$ compared to the pure V_2AlC also suggests that traces of Sc facilitates a change in stability, thus becoming more susceptible to HF etching. This is consistent with a recent report on $Nb_{1.33}CT_x$ derived from $(Nb_{2/3}Sc_{1/3})_2AlC$ where alloying Nb_2AlC with Sc causes a reduction of the etching time from 100 h to 30 h.[46]

The results from etching of $(V_{2/3}Sc_{1/2})_2AlC_{mix}$ in LiF + HCl is also shown in Fig. 4(a and b). The $(V_{2/3}Sc_{1/3})_2AlC$ i-MAX dissolved in less than 24 h, while V_2AlC and $(V_{2-x}Sc_x)_2AlC$ remained largely unaffected. After 144 h, the latter had turned into multilayered MXene. All impurity phases appear dissolved after both HF and LiF + HCl etching. A summary of conditions and morphologies observed is given in Table 1. The low angle (<10°) (002) peak from multilayered MXene, see Fig. 4(b), is present in both the HF and LiF + HCl treated material. All diffractograms show broadening and shift of the (002) peak to lower diffraction angles, see Fig. 4(b), consistent with a change in *c* lattice parameter (*c*-LP) for multilayer- and/or delaminated MXenes. The lower angle peak seen in the HF scan is multilayered MXene with traces of its respective T_x group and H_2O between MXene layers, giving rise to increased *c*-LP from 6.6 Å to 19.4 Å. The TBAOH data shows further delamination of the HF treated material using TBAOH intercalation and H_2O cleaning, further expanding the *c*-LP between layers from 19.4 Å to 30.3 Å. Likewise the LiF + HCl scan shows an increase in *c*-LP due to its respective T_x group and H_2O intercalation after cleaning, in line with previous reports.[45,47]

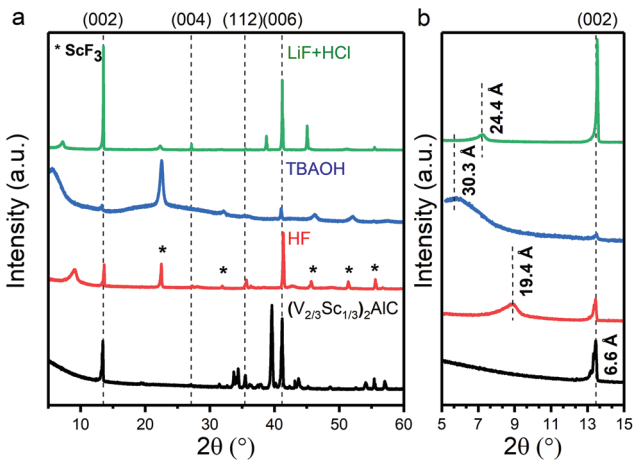

Fig. 4 (a) Full range XRD pattern of $(V_{2/3}Sc_{1/2})_2AlC_{mix}$ before etching, after etching in HF, after etching in HF followed by TBAOH intercalation and delamination, and after etching in LiF + HCl. (b) Same as (a) but focusing on 5–15° range showing shift in *c*-LP. High intensity peaks of V_2AlC in (a) are marked with a dashed line, and peaks originating from ScF_3, an impurity after etching, are marked with a star.

Previous reports also show synthesis of V_2CT_x through etching of V_2AlC with NaF + HCl at 90 °C for 72 h.[48] Attempts to use this method for $(V_{2/3}Sc_{1/3})_2AlC_{mix}$ was initiated, though the material deteriorated completely within 30 min after 9 h of etching with only V_2AlC remaining. This suggests a cascading decomposition of the phase.

Overview STEM and HRSTEM of LiF + HCl etched and, what appears to be, at least partly delaminated MXene in the form of scrolls is seen in Fig. 5(a–c). Assuming that the parent material is $(V_{2-x}Sc_x)_2AlC$, the resulting MXene is $V_{2-x}C$. Attempts to delaminate the material further was done by increasing the TBAOH content, and use more excessive mixing and prolonged sonication, though with no evidence for MXene scrolls with less than three layers. This suggests that a scroll could be a single layer MXene flake, with multilayer appearance due to rolling. The formation may be explained by the slow etching process of LiF + HCl, taking 144 h, in combination with an added reactivity caused by formation of Sc vacancies, which force the flakes to scroll.

A difference in surface chemistry from choice of etchant may also contribute to the scroll formation, though this needs to be further investigated. The same material etched in HF showed the traditional single-sheet MXene in HRSTEM, see

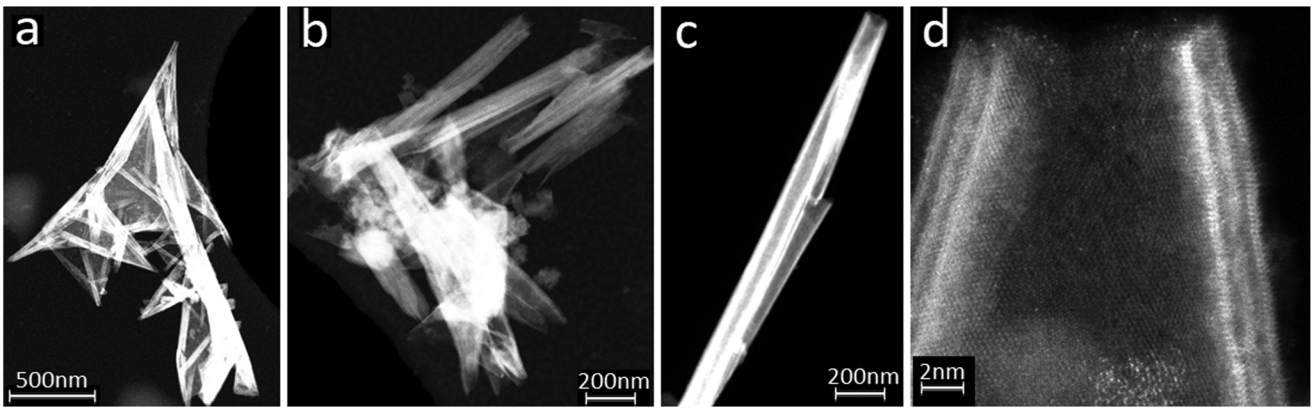

Fig. 5 Overview STEM images on scrolls of $V_{2-x}C$ MXene from etching in LiF + HCl for 144 h showing (a) and (b) clusters, (c) a single scroll, and (d) HRSTEM showing cross section of single scroll with three MXene layers.

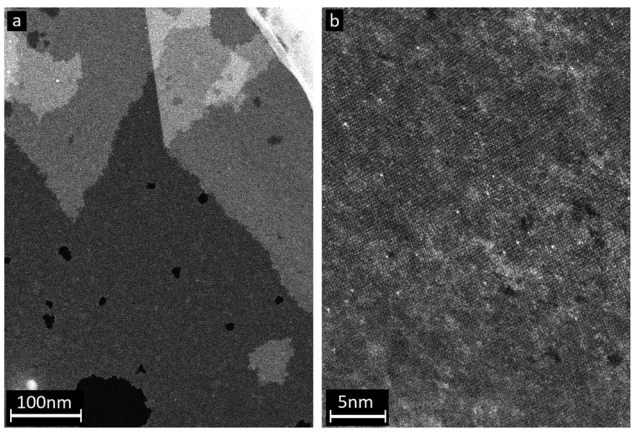

Fig. 6 STEM images on single sheet $V_{2-x}C$ MXene etched in HF for 24 h showing (a) distinct layering of multiple sheets and (b) close-up view showing signs of larger holes.

Fig. 6(a and b). It is important that the HF-treated material was only etched for 24 h, as opposed to 90 h required for V_2AlC to form MXene.[45] Altogether, the results show that (i) traces of Sc in V_2AlC significantly reduces the time required for MXene synthesis using HF, and (ii) LiF + HCl in combination with formation of Sc vacancies changes the MXene morphology to scrolls.

The observed large difference in time required for etching V_2AlC and $(V_{2-x}Sc_x)_2AlC$ provides a new path towards optimization and up-scaling of MXene synthesis. The origin of the reduced stability upon Sc incorporation may be an increased strain energy within the M-layer upon incorporation of the larger Sc atom (compared to V). It may also be possible that the Sc atoms are, again due to size, slightly shifter towards the A-layer, in line with the observations for i-MAX phases. This would also facilitate the MXene formation. We suggest that the same approach may be used for other MAX phases, *i.e.* to incorporate a small amount of Sc (or potentially some other element) to make the material more susceptible to etching. Furthermore, the control of morphology by simply changing etchant and introducing small amounts of impurities increases the range of potential applications. Using MXene scrolls could, for example, significantly improve the electrochemical performance and out-perform flat-sheet MXene or MXene mixed with interlayer spacers.

Conclusions

We have synthesized a new i-MAX phase, $(V_{2/3}Sc_{1/2})_2AlC$, with the characteristic in-plane chemical ordering identified from STEM-EDX. Even though this phase dissolves under a strongly exothermic reaction for the here applied etchants, we show that a solid solution of $(V_{2-x}Sc_x)_2AlC$ ($x \leq 0.05$) realize single sheets of $V_{2-x}C$ MXene or MXene scrolls from etching in HF or LiF + HCl, respectively. Furthermore, we show that the etching time in HF is reduced from 90 to 24 h by introducing a small amount of Sc in the V_2AlC. The observation that Sc can facilitate both optimized MXene synthesis procedures and control of the MXene morphology, may be an approach relevant for other MAX phases and their MXenes, for upscaling as well as property tuning.

Conflicts of interest

There are no conflicts to declare.

Acknowledgements

J. R. and P. P. acknowledge support from the Swedish Foundation for Strategic Research (SSF) for project funding (EM16-0004) and the Research Infrastructure Fellow program no. RIF 14-0074, and from the Knut and Alice Wallenberg (KAW) Foundation for a fellowship grant and project funding (KAW 2015.0043). All authors also acknowledge support to the Linköping Electron Microscopy Laboratory (KAW), and from the Swedish Government Strategic Research Area in Materials

Science on Functional Materials at Linköping University (Faculty Grant SFO-Mat-LiU No. 2009 00971). The Swedish Research council is also gratefully acknowledged through projects 642-2013-8020 and 2016-04412.

References

1 R. Mas-Balleste, C. Gomez-Navarro, J. Gomez-Herrero and F. Zamora, *Nanoscale*, 2011, **3**, 20–30.
2 K. J. Koski and Y. Cui, *ASC Nano*, 2013, **7**, 3739–3743.
3 B. Luo, G. Liu and L. Wang, *Nanoscale*, 2016, **8**, 6904–6920.
4 M. Naguib, M. Kurtoglu, V. Presser, J. Lu, J. Niu, M. Heon, L. Hultman, Y. Gogotsi and M. W. Barsoum, *Adv. Mater.*, 2011, **23**, 4248–4253.
5 M. Naguib, O. Mashtalir, J. Carle, V. Presser, J. Lu, L. Hultman, Y. Gogotsi and M. W. Barsoum, *ACS Nano*, 2012, **6**, 1322–1331.
6 P. Urbankowski, B. Anasori, T. Makaryan, D. Er, S. Kota, P. L. Walsh, M. Zhao, V. B. Shenoy, M. W. Barsoum and Y. Gogotsi, *Nanoscale*, 2016, **8**, 11385–11391.
7 R. Meshkian, L.-Å. Näslund, J. Halim, J. Lu, M. W. Barsoum and J. Rosen, *Scr. Mater.*, 2015, **108**, 147–150.
8 M. Alhabeb, K. Maleski, T. S. Mathis, A. Sarycheva, C. B. Hatter, S. Uzun, A. Levitt and Y. Gogotsi, *Angew. Chem.*, 2018, **130**, 5542–5546.
9 M. W. Barsoum, *MAX phases: properties of machinable ternary carbides and nitrides*, John Wiley & Sons, 2013.
10 M. W. Barsoum, *Prog. Solid State Chem.*, 2000, **28**, 201–281.
11 B. Anasori, M. R. Lukatskaya and Y. Gogotsi, *Nat. Rev. Mater.*, 2017, **2**, 16098.
12 M. Ghidiu, M. R. Lukatskaya, M.-Q. Zhao, Y. Gogotsi and M. W. Barsoum, *Nature*, 2014, **516**, 78.
13 J. Halim, M. R. Lukatskaya, K. M. Cook, J. Lu, C. R. Smith, L.-Å. Näslund, S. J. May, L. Hultman, Y. Gogotsi and P. Eklund, *Chem. Mater.*, 2014, **26**, 2374–2381.
14 F. Shahzad, M. Alhabeb, C. B. Hatter, B. Anasori, S. M. Hong, C. M. Koo and Y. Gogotsi, *Science*, 2016, **353**, 1137–1140.
15 M. Han, X. Yin, H. Wu, Z. Hou, C. Song, X. Li, L. Zhang and L. Cheng, *ACS Appl. Mater. Interfaces*, 2016, **8**, 21011–21019.
16 H. Liu, C. Duan, C. Yang, W. Shen, F. Wang and Z. Zhu, *Sens. Actuators, B*, 2015, **218**, 60–66.
17 M. Radovic and M. W. Barsoum, *Am. Ceram. Soc. Bull.*, 2013, **92**, 20–27.
18 J. Halim, K. M. Cook, M. Naguib, P. Eklund, Y. Gogotsi, J. Rosen and M. W. Barsoum, *Appl. Surf. Sci.*, 2016, **362**, 406–417.
19 I. Persson, L.-Å. Näslund, J. Halim, M. W. Barsoum, V. Darakchieva, J. Palisaitis, J. Rosen and P. O. Å. Persson, *2D Mater.*, 2017, **5**, 015002.
20 Q. Peng, J. Guo, Q. Zhang, J. Xiang, B. Liu, A. Zhou, R. Liu and Y. Tian, *J. Am. Chem. Soc.*, 2014, **136**, 4113–4116.
21 S. Shah, T. Habib, H. Gao, P. Gao, W. Sun, M. Green and M. Radovic, *Chem. Commun.*, 2017, **53**, 400–403.
22 V. Natu, M. Clites, E. Pomerantseva and M. W. Barsoum, *Mater. Res. Lett.*, 2018, **6**, 230–235.
23 M. Hu, Z. Li, H. Zhang, T. Hu, C. Zhang, Z. Wu and X. Wang, *Chem. Commun.*, 2015, **51**, 13531–13533.
24 M. Q. Zhao, C. E. Ren, Z. Ling, M. R. Lukatskaya, C. Zhang, K. L. Van Aken, M. W. Barsoum and Y. Gogotsi, *Adv. Mater.*, 2015, **27**, 339–345.
25 E. Kayali, A. VahidMohammadi, J. Orangi and M. Beidaghi, *ACS Appl. Mater. Interfaces*, 2018, **10**, 25949–25954.
26 Y. Cao, X. Li, I. A. Aksay, J. Lemmon, Z. Nie, Z. Yang and J. Liu, *Phys. Chem. Chem. Phys.*, 2011, **13**, 7660–7665.
27 Q. Qu, S. Yang and X. Feng, *Adv. Mater.*, 2011, **23**, 5574–5580.
28 M.-Q. Zhao, Q. Zhang, J.-Q. Huang, G.-L. Tian, J.-Q. Nie, H.-J. Peng and F. Wei, *Nat. Commun.*, 2014, **5**, 3410.
29 J. Zhu, H. Zhang and N. A. Kotov, *ACS Nano*, 2013, **7**, 4818–4829.
30 F. Meng, Y. Zhou and J. Wang, *Scr. Mater.*, 2005, **53**, 1369–1372.
31 J. Rosén, M. Dahlqvist, S. Simak, D. McKenzie and M. Bilek, *Appl. Phys. Lett.*, 2010, **97**, 073103.
32 A. S. Ingason, A. Mockuté, M. Dahlqvist, F. Magnus, S. Olafsson, U. B. Arnalds, B. Alling, I. A. Abrikosov, B. Hjörvarsson and P. Å. Persson, *Phys. Rev. Lett.*, 2013, **110**, 195502.
33 D. Horlait, S. C. Middleburgh, A. Chroneos and W. E. Lee, *Sci. Rep.*, 2016, **6**, 18829.
34 M. Nechiche, V. Gauthier-Brunet, V. Mauchamp, A. Joulain, T. Cabioc'h, X. Milhet, P. Chartier and S. Dubois, *J. Eur. Ceram. Soc.*, 2017, **37**, 459–466.
35 J. Rosen, P. Å. Persson, M. Ionescu, A. Kondyurin, D. McKenzie and M. Bilek, *Appl. Phys. Lett.*, 2008, **92**, 064102.
36 Z. Liu, L. Zheng, L. Sun, Y. Qian, J. Wang and M. Li, *J. Am. Ceram. Soc.*, 2014, **97**, 67–69.
37 B. Anasori, M. Dahlqvist, J. Halim, E. J. Moon, J. Lu, B. C. Hosler, E. a. N. Caspi, S. J. May, L. Hultman, P. Eklund, J. Rosén and M. W. Barsoum, *J. Appl. Phys.*, 2015, **118**, 094304.
38 Q. Tao, M. Dahlqvist, J. Lu, S. Kota, R. Meshkian, J. Halim, J. Palisaitis, L. Hultman, M. W. Barsoum and P. O. Persson, *Nat. Commun.*, 2017, **8**, 14949.
39 M. Dahlqvist, J. Lu, R. Meshkian, Q. Tao, L. Hultman and J. Rosen, *Sci. Adv.*, 2017, **3**, e1700642.
40 J. Lu, A. Thore, R. Meshkian, Q. Tao, L. Hultman and J. Rosén, *Cryst. Growth Des.*, 2017, **17**, 5704–5711.
41 R. Meshkian, M. Dahlqvist, J. Lu, B. Wickman, J. Halim, J. Thörnberg, Q. Tao, S. Li, S. Intikhab and J. Snyder, *Adv. Mater.*, 2018, **30**, 1706409.
42 L. Chen, M. Dahlqvist, T. Lapauw, B. Tunca, F. Wang, J. Lu, R. Meshkian, K. Lambrinou, B. Blanpain and J. Vleugels, *Inorg. Chem.*, 2018, **57**, 6237–6244.

43 M. Dahlqvist, A. Petruhins, J. Lu, L. Hultman and J. Rosen, *ACS Nano*, 2018, **12**, 7761–7770.
44 I. Persson, A. El Ghazaly, Q. Tao, J. Halim, S. Kota, V. Darakchieva, J. Palisaitis, M. W. Barsoum, J. Rosen and P. O. Persson, *Small*, 2018, **14**, 1703676.
45 M. Naguib, J. Halim, J. Lu, K. M. Cook, L. Hultman, Y. Gogotsi and M. W. Barsoum, *J. Am. Chem. Soc.*, 2013, **135**, 15966–15969.
46 J. Halim, J. Palisaitis, J. Lu, J. Thörnberg, E. Moon, M. Precner, P. Eklund, P. Å. Persson, M. Barsoum and J. Rosen, *ACS Appl. Nano Mater.*, 2018, **1**, 2455–2460.
47 Z.-h. Liu, Z.-M. Wang, X. Yang and K. Ooi, *Langmuir*, 2002, **18**(12), 4926–4932.
48 F. Liu, J. Zhou, S. Wang, B. Wang, C. Shen, L. Wang, Q. Hu, Q. Huang and A. Zhou, *J. Electrochem. Soc.*, 2017, **164**, A709–A713.